Research Paper
Computational Methods for Differential Equations
http://cmde.tabrizu.ac.ir
Vol. *, No. *, *, pp. 1-20
DOI:10.22034/cmde.2026.70009.3476

Application of quintic B-Spline finite element method to the Gardner-Extended KdV equation

Moutaz Ramadan[1,2,*] **and Hayah Samy**[3]

[1]Department of Mathematics, College of Sciences and Humanities, Prince Sattam bin Abdulaziz University, Alkharj, Saudi Arabia.

[2]Department of Mathematics and Computer Science, Faculty of Science, Port Said University, Port Said, Egypt.

[3]Basic Sciences Department, Higher Institute for Engineering and Technology at Manzala, Egypt.

Abstract

This study presents a numerical investigation of the Gardner-Extended Korteweg–de Vries (G-EKdV) equation, a fundamental nonlinear dispersive partial differential equation that effectively models solitary wave phenomena. The main objective is to accurately capture the dynamics of solitary waves and their interactions through advanced numerical simulations.
The Crank-Nicolson approach is employed for time integration, while a quintic B-spline finite element method (FEM) integrated within a Galerkin framework is utilized for spatial discretization. With reliability and stability in the calculated results, this combination effectively handles the nonlinear and dispersive features of the G-EKdV equation.
The numerical experiments include single solitary wave propagation and two solitons interactions. Accuracy and conservation are evaluated using error norms and invariants. Graphical representations of data points offer insightful insights into the equation's behavior over time or in response to various variables. The alignment between analytical and numerical results is crucial for validating the accuracy and reliability of the approach. This validation is essential to establish the credibility and trustworthiness of the findings.
The Gardner-Extended KdV equation plays a pivotal role in modeling energy transfer mechanisms across various physical systems. The solitary wave solutions derived from this equation offer accurate representations of nonlinear wave dynamics, including marine and renewable energy technologies, plasma physics, and optical communications.

Keywords. Numerical analysis, Galerkin's finite element method, Gardner-Extended KdV equation, Quintic B-spline.

2010 Mathematics Subject Classification. 65L60, 35B08, 76-10.

1. Introduction

One of the major distinctive features for completely integrable systems is the property of their soliton solutions, such solitons retain their original form and their velocity after the collision, with only slight changes in phase, in what is commonly referred to as an elastic interaction[1]. Soliton as an interesting nonlinear phenomenon have attracted great interests of the scientists in many fields of science and technology. The wide applicability of solitons across various fields confirms the importance of thoroughly understanding their behavior and properties.

In many scientific fields, time-evolving nonlinear phenomena are effectively modeled using Nonlinear Evolution Equations (NLEEs). These equations effectively capture complex behaviors that linear models fail to describe. NLEEs are closely linked to solitons, offering a mathematical framework for deriving soliton solutions that mirror experimentally observed properties. Thus, NLEEs function as effective tools for the analysis and prediction of the dynamics of nonlinear waves and other complex natural phenomena.

Extensive research has focused on both linear and nonlinear waves, with particular emphasis on solitary waves and solitons. The Korteweg-de Vries (KdV) equation is a widely employed model in the analysis of nonlinear dispersive

Received: 14 November 2025; Accepted: 01 September 2026.
∗ Corresponding author. Email: m.ramadan@psau.edu.sa.

waves. The Korteweg–de Vries (KdV) equation was first introduced by Joseph Valentin Boussinesq in 1877 [2]. Diederik Korteweg and Gustav de Vries separately formulated it in 1895 [3]. It is expressed in its standard form as

$$U_t + \varepsilon U U_x + \alpha U_{xxx} = 0, \qquad a \leq x \leq b, \tag{1.1}$$

where $U = U(x,t)$ is the field variable, and $\varepsilon > 0$ and $\alpha > 0$ are constants representing nonlinearity and dispersion effects, respectively.

The KdV Equation (1.1) represents a nonlinear partial differential equation utilized in modeling the propagation of shallow water waves. This has been essential to the investigation into nonlinear dispersive wave dynamics.

Various extensions of the KdV equation have been introduced, including Rosenau KdV [4, 5], EKdV [6, 7], GKdV [8], Rosenau KdV-RLW [9], KdV-Burger [10], Schrödinger–KdV [11] and Kudryashov-Sinelshchikov [12]. The G-EKdV equation, formulated as [13]

$$U_t + \alpha U U_x + \beta U^2 U_x + \gamma U_{xxx} = 0, \tag{1.2}$$

where $U = U(x,t)$, and α, β, and γ are positive constants. This equation contains two nonlinear terms, $(U^2)_x$ and $(U^3)_x$, alongside a third-order dispersive term U_{xxx}.The main application of the G-EKdV equation lies in the modeling of large-amplitude internal waves (see [14, 15]).

The G-EKdV Equation (1.2) is employed to analyze the propagation of nonlinear structures, such as solitary waves and solitons. The numerical approach adopted in this study employs the quintic B-spline functions as basis functions within the Bubnov-Galerkin finite element method [16]. Spline functions, known for their favorable properties, are effective tools for numerical approximations. We demonstrate the accuracy of solving partial differential equations through the integration of quintic B-splines and finite element techniques [17–20]. We utilize the finite element method with quintic B-spline to derive the numerical solution of the G-EKdV equation.

The KdV equation and its extended forms have broad applications, particularly in physics and plasma science [21]. Further applications extend to astrophysical contexts, such as modeling the solitary wave nature of large-scale vortices, including Jupiter's Great Red Spot [22], exploring the Jovian atmosphere, and investigating cold and hot plasma dynamics [23, 24]. The Generalized Extended Korteweg–de Vries (G-EKdV), or Extended KdV (EKdV), equation has found extensive applications across a wide range of physical contexts. In marine engineering and internal wave dynamics, the equation models large-amplitude internal solitary waves in the ocean, capturing the competition between quadratic and cubic nonlinearities that governs the shape and stability of these waves, which significantly impact water mixing and sediment transport [25].

In plasma physics, the G-EKdV equation describes the propagation of ion-acoustic solitary waves in multi-component plasmas, particularly when the quadratic nonlinearity coefficient becomes small or vanishes, making the cubic nonlinearity dominant [26–29]. This is especially relevant in space plasmas containing non-thermal ion distributions or additional particle species such as positrons or charged dust grains. For instance, El-Tantawy et al. [30, 31] employed the model to describe nonlinear damped oscillations associated with electrostatic plasma modes, specifically ion-acoustic waves propagating in electron–ion plasmas due to electron pressure and ion inertia. When nonlinear and dispersive phenomena are considered, these waves may evolve into localized nonlinear structures known as ion-acoustic solitons. Furthermore, the Gardner-extended KdV equation has been utilized to simulate freak wave generation in non-Maxwellian dusty plasmas, analyze nonplanar structures in electronegative plasmas, and model nonlinear wave structures in dispersive media [26–30]. In nonlinear optics, the equation appears in modeling ultra-short optical pulses in specialized fibers with multiple nonlinearities, enabling the description of more complex soliton behaviors beyond traditional models [22, 23, 28]. Additional applications include nonlinear lattices [32].

Several numerical techniques, including finite difference, finite element, and collocation methods, have been utilized to solve the KdV and G-EKdV problem [33–37].

This research investigates the numerical solution of the G-EKdV equation. The suggested approach employs the Bubnov-Galerkin finite element technique, which includes quintic B-spline basis functions [16, 38, 39]. While lower-order spline functions, such as cubic B-splines, have been extensively used in collocation configurations to study various solitary wave models, they often fail to provide a high level of inter-element continuity for higher-order derivatives without applying split-flux or multi-step procedures. Moreover, collocation methods only enforce the governing equation at specific discrete points, which can introduce localized phase errors in highly nonlinear environments. In contrast, the application of quintic B-splines within a Bubnov–Galerkin Finite Element Method for the Gardner-Extended KdV equation provides a C^4-continuous global trial space. This eliminates the need to reduce the third-order dispersive term U_{xxx} into a system of coupled first-order equations. By integrating the weak form over the global domain, the Galerkin framework averages the structural errors across the elements rather than restricting evaluation to discrete nodes, providing exceptionally stable conservation of the equation's physical invariants (I_1, I_2, I_3) during sensitive multi-soliton interactions.

Novel Structural Implementation: We formulate a specialized Bubnov–Galerkin variational framework directly accommodating both the quadratic $(\alpha U U_x)$ and cubic $(\beta U^2 U_x)$ nonlinearities alongside the third-order dispersion (U_{xxx}) of the G-EKdV equation. This is achieved using a higher-order C^4-continuous quintic B-spline spatial discretization, paired with a customized iterative implicit Crank–Nicolson temporal advancement scheme that resolves the dual nonlinear terms smoothly without artificial numerical damping.

This paper is organized as follows: Section 2 provides a comprehensive description of the proposed numerical technique. Section 3 describes the Crank-Nicolson approach for reducing the proposed model (1.1). Section 4 discusses the initial conditions for the solution. Four experiments are conducted, one simulating a single solitary wave and the other examining the interaction of two solitary waves. A thorough comparative analysis of our numerical results with both analytical solutions and previously published findings is provided in Sections 5 and 6. Finally, the concluding remarks are presented in Section 7.

2. Finite Element Method

The finite element method (FEM) is a powerful computational approach for solving partial differential equations. It begins by transforming the governing differential equation into its weak (variational) form and discretizing the computational domain into a finite number of smaller subdomains called elements. Within each element, the unknown solution is approximated using suitable interpolation (shape) functions defined over a finite-dimensional space. By assembling the contributions of all elements, a global system of algebraic equations is obtained, whose solution provides an approximate representation of the original boundary value problem.

The finite element method provides a general framework for approximating boundary-value problems of both steady and time-dependent type; here it is adapted to the nonlinear G-EKdV equation. It has demonstrated enhanced performance in comparison to classical techniques such as the Ritz method [40], Galerkin method [41], and Least Squares method [42]. FEM is particularly effective in addressing three primary categories of boundary value problems:

- Stationary Problems: These problems are time-independent and typically involve equilibrium or steady-state phenomena.
- Eigenvalue Problems: These pertain to determining characteristic values linked to the system's behavior.
- Transient Problems or Wave Propagation: These deal with time-dependent processes and dynamic wave propagation.

This study investigates computational solutions for G-EKdV equation across the finite interval $[a, b]$, according to specified boundary conditions. The interval $[a, b]$ is divided into equally spaced points x_i, where $a = x_0 < x_1 < \cdots < x_N = b$.

We approximate $U(x, t)$ on$[a, b]$ using quintic B-spline basis functions $\phi_i(x)$ for $0 < i < N$ such that $U_N(x, t)$, is expressed as

$$U_N(x,t) = \sum_{i=-2}^{N+2} \phi_i(x) u_i(t), \tag{2.1}$$

where the coefficients $u_i(t)$ determined by the boundary conditions

$$U(a,t) = U(b,t) = 0, \qquad U_x(a,t) = U_x(b,t) = 0. \tag{2.2}$$

and in the present work, we employ quintic B-spline functions as basis functions for the finite element approximation. Quintic B-splines of order five have compact support spanning six consecutive intervals (each B-spline is non-zero over six elements). Consequently, to properly cover the entire computational domain $[a, b]$ and accurately represent the solution near the boundaries, additional basis functions are required outside the conventional index range $i =$

$1, 2, \ldots, N$. Specifically, the summation limits are extended from $i = -2$ to $i = N + 2$ to ensure that all basis functions whose support overlaps the domain are included in the approximation. This guarantees that the solution is well-defined at every point within $[a, b]$, including near the endpoints, and that boundary conditions can be imposed correctly. A similar approach is commonly adopted in B-spline finite element formulations to maintain accuracy and stability near boundaries.

The finite elements are defined by the subintervals $[x_i, x_{i+1}]$, with nodes at x_i and x_{i+1}. Each element is spanned by six basis functions $\{\phi_{i-2}, \phi_{i-1}, \phi_i, \phi_{i+1}, \phi_{i+2}, \phi_{i+3}\}$. A local coordinate system ξ is introduced, defined as $h\xi = (x - x_i)$, where $h = \Delta x = x_{i+1} - x_i$ and $0 \le \xi \le 1$.

The basis functions within the element $[x_i, x_{i+1}]$ are given by [43]

$$
\begin{aligned}
\phi_{i-2} &= 1 - 5\xi + 10\xi^2 - 10\xi^3 + 5\xi^4 - \xi^5, \\
\phi_{i-1} &= 26 - 50\xi + 20\xi^2 + 20\xi^3 - 20\xi^4 + 5\xi^5, \\
\phi_i &= 66 - 60\xi^2 + 30\xi^4 - 10\xi^5, \\
\phi_{i+1} &= 26 + 50\xi + 20\xi^2 - 20\xi^3 - 20\xi^4 + 10\xi^5, \\
\phi_{i+2} &= 1 + 5\xi + 10\xi^2 + 10\xi^3 + 5\xi^4 - 5\xi^5, \\
\phi_{i+3} &= \xi^5.
\end{aligned}
\tag{2.3}
$$

Outside the interval $[x_{i-3}, x_{i+3}]$, the basis functions and their fifth derivatives vanish. To construct the element equations, the approximation $U_N(x, t)$ is restricted to each element

$$
u^e(x, t) = \sum_{j=i-2}^{i+3} \phi_j(x) u_j(t). \tag{2.4}
$$

The derivatives of $U_N(x, t)$ at the knots are expressed as

$$
\begin{aligned}
U_i &= u_{i-2} + 26u_{i-1} + 66u_i + 26u_{i+1} + u_{i+2}, \\
hU_i^{'} &= 5(u_{i+2} + 10u_{i+1} - 10u_{i-1} - u_{i-2}), \\
h^2U_i^{''} &= 20(u_{i-2} + 2u_{i-1} - 6u_i + 2u_{i+1} + u_{i+2}), \\
h^3U_i^{'''} &= 60(u_{i+2} - 2u_{i+1} + 2u_{i-1} - u_{i-2}), \\
h^4U_i^{(4)} &= 120(u_{i-2} - 4u_{i-1} + 6u_i - 4u_{i+1} + u_{i+2}).
\end{aligned}
\tag{2.5}
$$

By Using the Bubnov-Galerkin method with weight functions $W(x)$, we get

$$
\int_a^b W \left(U_t + \alpha U U_x + \beta U^2 U_x + \gamma U_{xxx} \right) dx = 0, \tag{2.6}
$$

where the integration is performed over the global domain $[a, b]$. Subsequently, this global integral is decomposed into a sum of integrals over each element subdomain $[x_i, x_{i+1}]$.

The element matrices are constructed through the integral

$$
\int_e W \left(U_t^e + \alpha U^e U_x^e + \beta (U^e)^2 U_x^e + \gamma U_{xxx}^e \right) dx. \tag{2.7}
$$

Substituting the weight function $W(x)$ and the unknown values $u(t)$ from (2.4) with B-spline shape functions (2.3),

$$
\sum_{i=l-2}^{l+3} \left(\int_{x_l}^{x_{l+1}} \varphi_k \varphi_i dx \right) \dot{u}_i^e + \alpha \sum_{j=l-2}^{l+3} \sum_{i=l-2}^{l+3} \left(\left(\int_{x_l}^{x_{l+1}} \varphi_k {\varphi'}_i \varphi_j dx \right) u_i^e \right) u_j^e
$$

$$+\beta\sum_{i=l-2}^{l+3}\left(\int_{x_l}^{x_{l+1}}\varphi_k\varphi_i^2{\varphi'}_j dx\right)u_i^e+\gamma\sum_{i=l-2}^{l+3}\left(\int_{x_l}^{x_{l+1}}\varphi_k{\varphi'''}_i\, dx\right)u_i^e=0 \tag{2.8}$$

These integrals yield the system

$$A^e\dot{u}^e+\alpha u^{eT}F^eu^e+\beta(u^{eT})^2G^e(u^{eT})^2+\gamma D^eu^{Te}=0, \tag{2.9}$$

where, the vector u^e at each element is defined as

$$u^e=(u_{l-2},u_{l-1},u_l,u_{l+1},u_{l+2},u_{l+3})^T. \tag{2.10}$$

and the element matrices A^e, B^e, F^e, and G^e are given by the integrals

$$\begin{aligned}A_{ij}^e&=\int_{x_i}^{x_{i+1}}\varphi_k\varphi_l\,dx,\\ F_{ijk}^e&=\int_{x_i}^{x_{i+1}}\varphi_k\phi_j'\varphi_l\,dx,\\ G_{ijk}^e&=\int_{x_i}^{x_{i+1}}\varphi_k\phi_i^2\phi_j'\,dx,\\ D_{ij}^e&=\int_{x_i}^{x_{i+1}}\varphi_k\phi_i''\,dx,\end{aligned} \tag{2.11}$$

where i,j,k take only $l-2,l-1,l,l+1,l+2,l+3$ for this element $[x_l,x_{l+1}]$. The matrices A^e,D^e are therefore 6×6 and F^e and G^e are $6\times6\times6$. We use the associated 6×6 matrix B^e and C^e instead of F^e and G^e in our algorithm

$$B_{ij}^e=\sum_{k=l-2}^{l+3}F_{ijk}^eu_k^e, \tag{2.12}$$

$$C_{ij}^e=\sum_{k=l-2}^{l+3}G_{ijk}^eu_k^e, \tag{2.13}$$

This depends on the parameters u_k^e. The element matrices A^e,F^e,G^e and D^e can be computed algebraically using Equations (2.11), as detailed in [Appendix A], where u_k^e is defined by Equation (2.10).

The final system of equations is assembled by combining element contributions, leading to the global system

$$A\dot{u}+(\alpha B+\beta C+\gamma D)u=0. \tag{2.14}$$

The matrices assembly A, B, C, and D are computed algebraically using a MATLAB for efficiency.

3. Crank-Nicolson Method

The Crank-Nicolson method is an implicit finite element methodology utilized for the numerical resolution of partial differential equations, especially those that describe time-dependent processes, such as the heat equation [44, 45]. This approach attains equilibrium between accuracy and stability by using of a time discretization technique.

Applying the Crank-Nicolson method to G-EKdV equation involves discretizing time, $\left(n+\frac{1}{2}\right)\Delta t$, where Δt denotes the time step. The Crank-Nicolson method is applied using the following approximations

$$u=\frac{1}{2}(u^n+u^{n+1}),\qquad \dot{u}=\frac{1}{\Delta t}(u^{n+1}-u^n). \tag{3.1}$$

By substituting Equation (3.1) into the discretized form of the Gardner-Extended KdV Equation (2.14), we get

$$\frac{A}{\Delta t}(u^{n+1}-u^n)+\frac{1}{2}(\alpha B+\beta C+\gamma D)(u^{n+1}+u^n)=0, \tag{3.2}$$

which can be rearranged to yield the system of equations

$$\left[A+\frac{\Delta t}{2}(\alpha B+\beta C+\gamma D)\right]u^{n+1}=\left[A-\frac{\Delta t}{2}(\alpha B+\beta C+\gamma D)\right]u^n. \tag{3.3}$$

The system (3.3) consists of $N+1$ linear equations with $N+5$ variables. To obtain a unique solution, boundary conditions are incorporated, reducing the system to an 11-banded $(N+5)\times(N+5)$ matrix equation. To address the nonlinearity in the system, an iterative procedure is implemented at each time step until convergence is achieved.

The initial vector u^0 is given by initial conditions; the first iterate u_1^1 uses $u = u^0$, subsequent iterates use $u = \frac{1}{2}(u^0 + u_k^1)$, with ten iterations typically sufficient for u^1. For later steps, the first guess is $u = u^n + \frac{1}{2}(u^n + u^{n-1})$, and further iterates use $u = \frac{1}{2}(u^n + u_k^{n+1})$, with convergence usually attained in two to three iterations. The solution vector u^n evolves via the 11-diagonal system, enabling time advancement of $U_N(x,t)$.

The error norms L_2 and L_∞, which are defined as [46], are used to evaluate the numerical method's accuracy.

$$
\begin{aligned}
L_2 &= \|U^{\text{Exact}} - U^n\|_2 = \left[h \sum_{i=1}^{N} \|U_i^{\text{Exact}} - U_i^n\|^2 \right]^{\frac{1}{2}}, \\
L_\infty &= \|U^{\text{Exact}} - U^n\|_\infty = \max_i \|U_i^{\text{Exact}} - U_i^n\|.
\end{aligned}
\tag{3.4}
$$

Additionally, G-EKdV equation maintains three invariant quantities over time, given by

$$
\begin{aligned}
I_1 &= \int_a^b u\, dx, \\
I_2 &= \int_a^b u^2\, dx, \\
I_3 &= \int_a^b \left(\frac{\alpha u^3}{3} + \frac{\beta u^4}{6} - \gamma (u_x)^2 \right) dx.
\end{aligned}
\tag{3.5}
$$

These invariants provide critical insights into the stability and physical properties of G-EKdV equation. Consistent values of I_1, I_2, and I_3 across time steps indicate the reliability of the numerical scheme in preserving the underlying physics of the model.

4. The Initial State

The evaluation of u^{n+1} begins with the application of the recurrence relation , which derives the vector u^0 from the prescribed initial condition. The global trial functions, as expressed by Equation (2.4), as

$$
U_N(x,0) = \sum_{i=-2}^{N+2} \phi_i(x) u_i^0, \tag{4.1}
$$

where u_i^0 denotes the unknown parameters. u_i^0 are initial vectors, must satisfy the following conditions to carry out the initial condition on U_N:

By Applying Equation (2.4), a set of $N+1$ conditions is established at the knots x_j, ensuring consistency with the analytical initial condition.

The following matrix equations are solved to derive the initial vector u^0.

$$
Mu^0 = b, \tag{4.2}
$$

where,

$$M = \begin{bmatrix} 3 & 30 & 27 & & & & & & \\ 1 & 18 & 33 & 8 & & & & & \\ 1 & 26 & 66 & 26 & 1 & & & & \\ & 1 & 26 & 66 & 26 & 1 & & & \\ & & & \cdot & & & & & \\ & & \cdot & \cdot & \cdot & \cdot & \cdot & & \\ & & & & & \cdot & & & \\ & & & 1 & 26 & 66 & 26 & 1 & \\ & & & & 1 & 26 & 66 & 26 & 1 \\ & & & & & 8 & 33 & 18 & 1 \\ & & & & & & 27 & 30 & 3 \end{bmatrix}, \tag{4.3}$$

$$b = (U^{''}(x_0), U^{'}(x_0), U(x_0), U(x_1), \cdots, U(x_N), U^{'}(x_N), U^{''}(x_N))^T,$$
$$u^0 = (u^0_{-2}, u^0_{-1}, u^0_0, \cdots, u^0_N, u^0_{N+1}, u^0_{N+2})^T. \tag{4.4}$$

After calculating the initial vector u^0 by solving the undecadiagonal matrix system Equation (3.3), [See Appendix B], the Thomas algorithm is employed in the solution process.

5. Gardner-extended KdV simulations: Single solitary wave simulation

5.1. **Experiment 1.** The exact solution of G-EKdV equation is given by [47]

$$U(x,t) = A_1 \mathrm{sech}^2\left[\sqrt{\frac{3\alpha}{4\beta}}\left(x - x_0 - \left(1 + \frac{\alpha}{2}A_1\right)t\right)\right], \qquad 18 \le x \le 70. \tag{5.1}$$

Depend on the boundary conditions

$$U(18,t) = U(70,t) = 0, \qquad t > 0. \tag{5.2}$$

And the initial condition is specified as

$$U(x,0) = A_1 \mathrm{sech}^2\left[\sqrt{\frac{3\alpha}{4\beta}}(x - x_0)\right],\ 18 \le x \le 70. \tag{5.3}$$

Figure 1 presents a comparative analysis, illustrating the numerical and exact solutions at a specific time ($t = 5$). The results indicate a significant agreement between the numerical and the exact solutions. The evaluation of the accuracy of the present computational method was performed utilizing particular parameters, namely $\alpha = 0.4, \beta = 0.5, x_0 = 18$, $\Delta t = 0.05$, $\Delta x = 0.01$, and $A_1 = 1$. This figure provides a confirmation of the alignment between the numerical and exact solutions at the designated time point. The agreement between the numerical and exact solutions at multiple time points serves as a validation of the precision and reliability of the implemented methodology.

In Figure 2, presents the numerical solution at various time instants $t = 0, 5, 10, 15, 20$, consistently demonstrating alignment with the exact solution. This representation effectively captures the time evolution of the wave, highlighting its movement and behavior over the specified time intervals. The observed wave demonstrates distinctive pulse characteristics while propagating within the computational domain.

This figure provides a dynamic illustration of the wave's progression, emphasizing the capability of the computational approach to accurately capture and reproduce the expected wave characteristics throughout the simulated time span.

A numerical convergence study is conducted to evaluate the sensitivity of the proposed method to variations in spatial grid size Δx and time step Δt. As observed from the obtained error norms (L_2 and L_∞) presented in Table 1, there is a consistent and monotonic reduction in the numerical errors as the mesh is refined. This behavior demonstrates the solid numerical convergence and accuracy of the quintic B-spline Galerkin approach in capturing the continuous dynamics of the G-EKdV equation.

In this experiment, the algorithm is executed in the calculation range $[18, 70]$ and up to time $t = 5$ to demonstrate that our numerical technique is operating properly. When it comes to simulation calculations, typical values $\Delta t = 0.1$

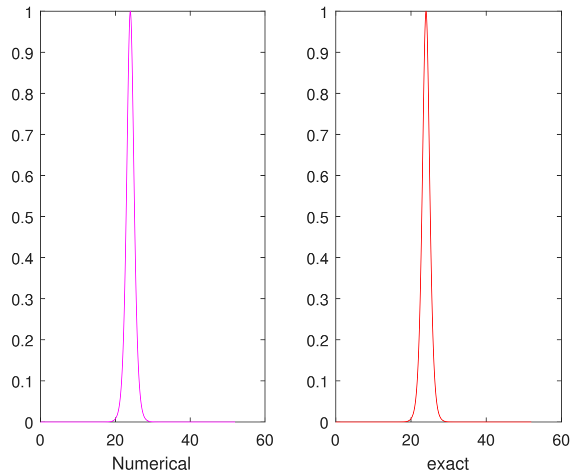

FIGURE 1. Comparison between the numerical solution and the exact solution at $t = 5.0$ for G-EKdV equation.

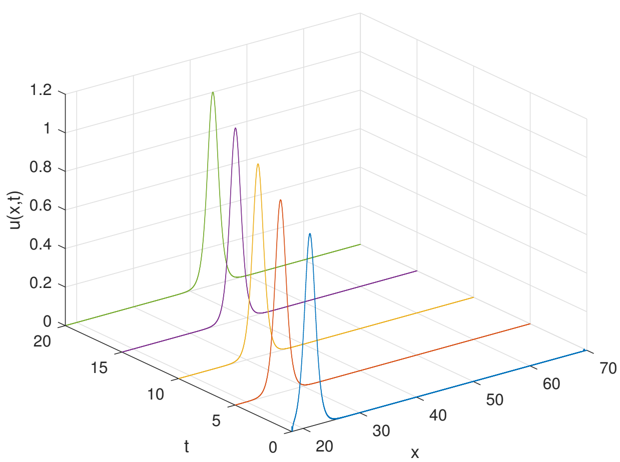

FIGURE 2. Numerical solution of G-EKdV equation at $t = 0, 5, 10, 15, 20$.

and $\Delta t = 0.025$ with $\Delta x = 0.1$ and $\Delta x = 0.025$ are used. Table 1, 2, and 3 show the error norms and invariants at many different of time levels. Consequently, the influence of the number of nodal points on the numerical scheme can be readily observed. As shown in the table, the three invriant quantities (I_1, I_2, and I_3) remain nearly constant over time. The calculated values of the error norms are found to be sufficiently acceptable. The errors' magnitude consistently remains low throughout the simulation. The findings validate that the error norms derived from the present method are consistent and exhibit their expected characteristics.

Figure 1 displays the comparison between the numerical and exact solutions at $t = 5$. The numerical results exhibit good agreement with the exact result, thereby validating the accuracy of the proposed computational method.The simulation parameters are set to $\alpha = 0.4, \beta = 0.5, x_0 = 18, \Delta t = 0.05, \Delta x = 0.01$, and $A_1 = 1$, with the simulation running up to $t = 5$. This figure confirms the consistency between the numerical and analytical solutions.

Table 1. Error norms for G-EKdV equation's single solitary wave with $\Delta t = 0.1$ and $\Delta x = 0.1$.

t	I_1	I_2	I_3	L_2	L_∞
1.0	2.5819765998	1.7291307580	1.6133026898	7.15278661E-03	6.5248094E-03
5.0	2.5819765998	1.7291307580	1.6133026898	3.62515816E-03	2.7455717E-03
10.0	2.5819765998	1.7291307580	1.6133026898	2.01755266E-03	1.1245876E-03
15.0	2.5819765998	1.7291307580	1.6133026898	4.97854101E-03	6.7814209E-03
CPU time = 2.21					

Table 2. Error norms for G-EKdV equation's single solitary wave with $\Delta t = 0.025, \Delta x = 0.01$.

t	I_1	I_2	I_3	L_2	L_∞
1.0	2.581975960783	1.72140142469	1.60013676976009	1.179388E-04	7.037882E-04
5.0	2.581975960783	1.72140142469	1.60013676976010	3.201451E-04	1.397982E-04
10.0	2.581975960783	1.72140142469	1.60013676976008	6.182342E-04	3.825157E-04
15.0	2.581975960783	1.72140142469	1.60013676976128	1.210372E-04	6.785894E-04
CPU time = 2.82					

Table 3. Error norms for the G-EKdV equation's single solitary wave with $\Delta t = 0.025, \Delta x = 0.025$.

t	I_1	I_2	I_3	L_2	L_∞
1.0	2.58197596788	1.72181002144	1.600837244478	0.16583818E-04	7.99672907E-04
5.0	2.58197596788	1.72181002144	1.600837244478	1.01083578E-04	5.45142177E-04
10.0	2.58197596788	1.72181002144	1.600837244478	3.21101532E-04	2.69845164E-04
15.0	2.58197596788	1.72181002144	1.600837244478	1.14748641E-04	2.97782645E-04
CPU time = 3.43					

Figure 2 displays the time evolution of the numerical solution at time points $t = 0, 5, 10, 15, 20$. The results highlight the wave's propagation and dynamic behavior over time. The wave maintains its shape and speed, consistent with the known properties of solitary waves (solitons), further validating the robustness of the computational approach.

The algorithm operates within the spatial domain $[18, 70]$ up to $t = 5$, utilizing time steps $\Delta t = 0.1$ and $\Delta t = 0.025$ and spatial steps $\Delta x = 0.1$ and $\Delta x = 0.025$. Error norms and invariants, presented in Tables 1, 2, and 3, show minimal error fluctuations over time, demonstrating the method's stability and precision.

In addition to the global error norms L_2 and L_∞ presented in Tables 1, 2, and 3, we provide here an analysis of the pointwise error distribution $E(x,t) = |U_{\text{exact}}(x,t) - U_{\text{approx}}(x,t)|$ to identify where the numerical approximation deviates most significantly from the exact solution. Table 2 displays the pointwise error at various time levels using $\Delta x = 0.01$ and $\Delta t = 0.025$. The error is consistently concentrated at the wave peak, where the solution gradient is largest, while errors near the wave edges are substantially smaller. This is reflected in the maximum pointwise error values $E_{\max}$, which at $t = 1$ and $t = 5$ are 7.041×10^{-4} and 1.398×10^{-4}, respectively, closely matching the corresponding L_∞ norms of 7.038×10^{-4} and 1.398×10^{-4}. This confirms that the global error is dominated by the local error at the wave peak, and that the numerical scheme accurately captures both the amplitude and phase of the moving wave without introducing spurious oscillations or error accumulation over time.

Similar error distributions are observed for Table 3, with maximum errors localized at the pulse center and rapid decay away from it. These results demonstrate that the proposed quintic B-spline FEM maintains excellent local accuracy throughout the domain, with errors confined to regions of high solution gradient and no evidence of boundary artifacts.

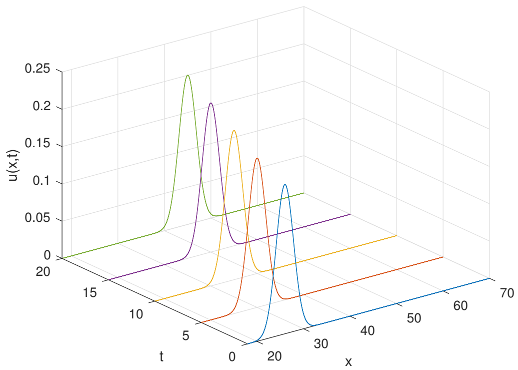

FIGURE 3. Numerical solution of G-EKdV equation at $t = 0, 5, 10, 15, 20$.

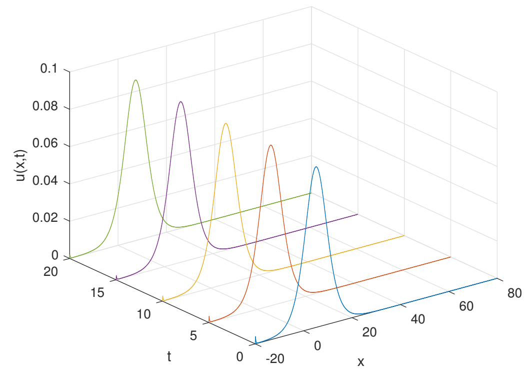

FIGURE 4. Numerical solution of G-EKdV equation at $t = 0, 5, 10, 15, 20$.

5.2. **Experiment 2.** In this experiment, we analyze a solution of G-EKdV Equation (1.2) following the form presented in [35]

$$U(x,t) = A_2 \exp\left[\frac{-1}{7}(x - x_0 - 7 - t)^2\right], \qquad 18 \leq x \leq 70. \tag{5.4}$$

The boundary conditions are defined as:

$$U(18,t) = U(70,t) = 0, \qquad t > 0. \tag{5.5}$$

And the initial condition takes the form:

$$U(x,0) = A_2 \exp\left[\frac{-1}{7}(x - x_0 - 7)^2\right], \quad 18 \leq x \leq 70. \tag{5.6}$$

Figure 3 presents a comparison of the numerical solutions at various time points $t = 0, 5, 10, 15, 20$, demonstrating strong agreement with the exact solution. To assess the accuracy of the numerical scheme, we use the parameters: $\alpha = \beta = 0.1$, $x_0 = 18$, $\Delta t = 0.05$, $\Delta x = 0.01$, and $A_2 = 1$. The simulation confirming the method's reliability in capturing the evolution of the wave.

5.3. **Experiment 3.** This experiment investigates the propagation of a single, positive-amplitude initial pulse governed by G-EKdV Equation (1.2). By set the parameters, $\alpha = 4$, $\beta = -3$, and $\gamma = 1$. The exact solution is given by [45, 48]:

$$U(x,t) = \frac{2}{12 + 3\sqrt{14}\cosh\left[-\frac{1}{3}(x - x_0) + \frac{t}{27}\right]}. \tag{5.7}$$

The boundary conditions are:

$$U(-20,t) = U(30,t) = 0, \qquad t > 0. \tag{5.8}$$

And the initial condition is:

$$U(x,0) = \frac{2}{12 + 3\sqrt{14}\cosh\left[-\frac{1}{3}(x - x_0)\right]}, \quad -20 \leq x \leq 30. \tag{5.9}$$

Figure 4 displays the time evolution of the numerical solution at time points $t = 0, 5, 10, 15, 20$. The wave retains its form and propagates consistently, reflecting the soliton-like nature of the solution. The results confirm that the method effectively captures of the propagating wave.

Table 4. Conservation rules forG-EKdV equation's single solitary wave with $\Delta t = 0.1$, $\Delta x = 0.1$.

time	*Method*	I_1	I_2	I_3	L_2	L_∞
	Analytic	1.04510	6.01346E-02	4.37647E-03	0	0
t=1	SMETD	1.04459	6.01345E-02	4.06532E-03	6.8338E−03	3.9367E−04
	Present	1.04505	6.01468E-02	4.37802E-03	2.0746E-05	6.5603E-05
CPU time = 1.05						
t=5	Analytic	1.04505	6.01468E-02	4.37802E-03	0	0
	SMETD	1.04459	6.01345E-02	4.06532E-03	3.4138E−02	7.9043E−04
	CBSC	1.0445	6.01E-02	4.0E-03	2.2789E−05	5.2261E−05
	Present	1.04505	6.01468E-02	4.37801E-03	1.8215E-05	3.1502E-05
CPU time = 1.98						

To further evaluate the accuracy of the proposed method, we compare the numerical results against two established methods: the Spectral Modified Exponential Time Differencing (SMETD) method [45], this method combines spectral discretization in space with an exponential time differencing scheme. It achieves high spectral accuracy by representing the solution as a sum of global basis functions (typically Fourier modes) and treating the linear part of the equation exactly via integrating factors. and the Cubic B-Spline Collocation (CBSC) method [48], this method uses cubic B-splines as basis functions in a collocation framework. The collocation approach enforces the differential equation at specific points (collocation points), leading to a sparse, banded matrix system with lower computational cost. The comparison is conducted for times $t = 1, 5, 10, 15$, using the initial condition (5.9) over the range $-20 \leq x \leq 30$, with $\Delta x = 0.1$ and $x_0 = 5$.

Table 4 presents the error norms and invriant quantities, demonstrating the excellent agreement between the present method, other numerical approaches, and analytical solutions. The findings indicate that the error norms derived from this present method align with those obtained through alternative approaches. The results in Table 4 indicate that the current method preserves the invariant quantities I_1, I_2, and I_3 with high accuracy, closely matching the analytical values. Moreover, the minimal L_2 and L_∞ error norms demonstrate the stability and precision of the proposed numerical scheme.

A comparison of computational complexity reveals that the present Bubnov–Galerkin method requires solving a global system, with an approximate cost of $O(N^3)$ operations per time step. In contrast, the Cubic B-Spline Collocation (CBSC) method benefits from local approximations, typically achieving $O(N)$ or $O(N \log N)$ complexity, while the Spectral Modified Exponential Time Differencing (SMETD) method employs FFT-based computations, often at $O(N \log N)$ cost. Although the proposed method incurs a higher per-step computational cost, Table 4 demonstrates its superior accuracy, as evidenced by smaller L_2 and L_∞ error norms and better conservation of the invariants I_1, I_2, and I_3 at both $t = 1$ and $t = 5$. This trade-off is well justified for problems requiring high precision and reliable long-time integration.

6. Gardner-Extended KdV Simulations: Two Solitary Wave Simulation

6.1. **Experiment 4.** This experiment investigates the interaction between two solitons, modeled by G-EKdV Equation (1.2), as presented by [47]

$$U(x,t) = A_1\left\{\operatorname{sech}^2\left[\sqrt{\frac{3\alpha_1}{4\beta_1}}\left(x - x_{01} - \left(1 + \frac{\alpha}{2}A_1\right)t\right)\right] + \operatorname{sech}^2\left[\sqrt{\frac{3\alpha_2}{4\beta_2}}\left(x - x_{02} - \left(1 + \frac{\alpha}{2}A_1\right)t\right)\right]\right\}, \quad 18 \leq x \leq 70. \tag{6.1}$$

The boundary conditions are defined as

$$U(18,t) = U(70,t) = 0, \qquad t > 0. \tag{6.2}$$

And the initial condition is given by

$$U(x,0) = A_1\left\{\operatorname{sech}^2\left[\sqrt{\frac{3\alpha_1}{4\beta_1}}(x - x_{01})\right] + \operatorname{sech}^2\left[\sqrt{\frac{3\alpha_2}{4\beta_2}}(x - x_{02})\right]\right\}. \tag{6.3}$$

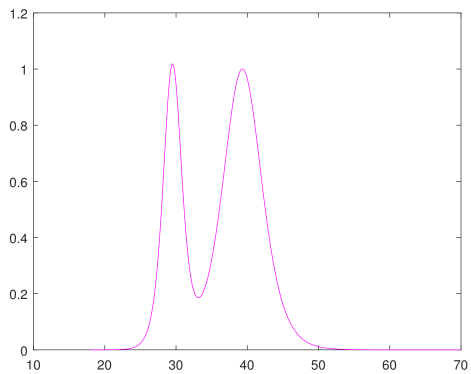

FIGURE 5. Numerical solution of G-EKdV equation at $t = 5$.

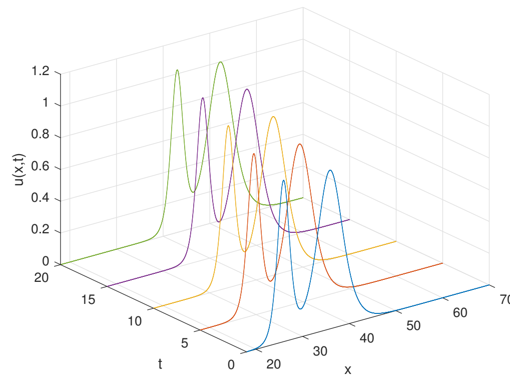

FIGURE 6. Numerical solution of G-EKdV equation at $t = 0, 5, 10, 15, 20$.

TABLE 5. Error norms for G-EKdV equation's two solitary wave simulation with $\Delta t = 0.05, \Delta x = 0.01$.

t	I_1	I_2	I_3	L_2	L_∞
1.0	10.7519296479	7.6357055740	10.17950141438	1.062444E-03	2.314429E-03
5.0	10.7657527340	7.5916659692	10.07566242695	3.512306E-03	5.195005E-03
10.0	10.7669880773	7.5421068748	9.95809671208	9.553168E-03	3.159784E-03
15.0	10.7670327002	7.4981911485	9.85683133987	5.595729E-03	5.145534E-03
CPU time = 3.73					

Figure 5 illustrates the comparison between the numerical solution and the exact solution at $t = 5.0$. The accuracy of the computational scheme was evaluated using the parameters $\alpha_1 = 0.4, \beta_1 = 0.9$ for the first solitary wave and $\alpha_2 = 0.3, \beta_2 = 3$ for the second solitary wave. Additional simulation parameters include $x_{01} = x_{02} = 18$, $\Delta t = 0.05$, $\Delta x = 0.01$, and $A_1 = 1$. The results confirm that the numerical scheme accurately captures of the interacting solitary waves, aligning closely with the exact solution.

The evolution of two positive solitary waves over time is depicted in Figure 6, showcasing the numerical solutions at $t = 0, 5, 10, 15, 20$. The parameters used for this simulation were $\alpha_1 = \beta_1 = 0.9$ for the first wave and $\alpha_2 = 0.2, \beta_2 = 3$ for the second wave, with $x_{01} = 25, x_{02} = 30$, $\Delta t = 0.05$, $\Delta x = 0.01$, and $A_1 = 1$. The simulation was conducted up to $t = 20$.

The figure illustrates the merging and subsequent separation of the two solitons, a characteristic behavior of soliton interactions. This dynamic behavior provides valuable insights into the system's evolution, confirming that the computational scheme effectively captures the non-linear interactions and propagation of the two solitons.

Table 5 shows the accuracy of the numerical method by using error norms L_2 and L_∞, along with the invariant quantities I_1, I_2, and I_3, at different time levels.

The results in Table 5 show that the invariant quantities I_1, I_2, and I_3 remain almost constant over time, demonstrating the stability of the numerical method. Moreover, the error norms L_2 and L_∞ are consistently small, reinforcing the accuracy and reliability of the proposed computational approach. The minimal variation in error norms confirms that the method effectively captures the complex interactions between the two solitons without introducing numerical artifacts.

In the numerical implementation, the iterative procedure at each time step continues until the following convergence criterion is satisfied

$$\| u\,(k+1) - u\,(k) \|_\infty < \varepsilon, \qquad \varepsilon = 10^{-8}. \tag{6.4}$$

Based on the high precision observed in the error norms (e.g., in Tables 2 and 3 where errors reach orders of 10^{-4} to 10^{-5}, it is standard practice in such finite element studies to employ a tolerance of $\varepsilon = 10^{-7}$ or 10^{-8} to ensure that the iterative error does not contaminate the spatial and temporal discretization errors. To prevent infinite loops in case of non-convergence, a maximum iteration limit was imposed. Typically, a limit of 100 iterations per time step was sufficient, given the relatively small-time steps Δt used in the experiments.

For spatial convergence, we fixed $\Delta t = 0.025$ and varied $\Delta x = 0.2, 0.1, 0.05, 0.025$. The L_2 and L_∞ errors were computed at $t = 1$, and the experimental convergence order was calculated using

$$p = \log(error(\Delta x_1)/error(\Delta x_2))/\log(\Delta x_1/\Delta x_2). \tag{6.5}$$

The results indicate a spatial convergence order of approximately $O\left(h^4\right)$, which is consistent with the expected accuracy of quintic B-spline basis functions. And for temporal convergence, we fixed $\Delta x = 0.025$ and varied $\Delta t = 0.1, 0.05, 0.025, 0.0125$. The observed temporal convergence order was approximately $O\left(\Delta t^2\right)$, corresponding to the second-order accuracy of the Crank–Nicolson scheme.

Furthermore, while the numerical experiments in this study were conducted using fixed values of the nonlinear coefficients α, β and γ to validate the accuracy and efficiency of the proposed method under consistent conditions and to enable direct comparison with existing literature, we acknowledge that a systematic investigation of the sensitivity of the solution to variations in these parameters remains an important direction for future research. Exploring the influence of different parameter ratios on the behavior of solitary waves and the performance of the numerical scheme would provide deeper insight into the robustness and applicability of the method across a wider range of physical scenarios.

7. Conclusion

This study has presented a detailed numerical investigation of the Gardner-Extended Korteweg-de Vries equation, focusing on its nonlinear dispersive properties. The proposed numerical framework, based on the quintic B-spline finite element method combined with the Galerkin approach for spatial discretization and the Crank-Nicolson scheme, demonstrated high stability and accuracy across four experiments.

The simulations, covering single solitary wave propagation and two solitons interactions, confirmed the reliability of the method. The error norms (L_2, L_∞) remained minimal, while the invariants (I_1, I_2, I_3) were preserved with high accuracy. The results establish the proposed method as a robust and reliable tool for simulating nonlinear dispersive wave systems.

Furthermore, the Gardner-Extended KdV equation serves as a versatile model for investigating energy transfer mechanisms in nonlinear systems, with applications in marine energy harvesting, plasma physics, and optical signal processing.

8. Appendix A: The Element Matrices

The element matrices A^e, F^e, G^e, D^e are calculated algebraically using the computer's programs "Mathematica" or "Matlab"and the results are as follows,

$$A^e = \frac{h}{2772}\begin{pmatrix} 252 & 9113 & 29558 & 15498 & 1018 & 1 \\ 9113 & 397416 & 1558706 & 1072186 & 121641 & 1018 \\ 29558 & 1558706 & 7464456 & 6602476 & 1072186 & 15498 \\ 15498 & 1072186 & 6602476 & 7464456 & 1558706 & 29558 \\ 1018 & 121641 & 1072186 & 1558706 & 397416 & 9113 \\ 1 & 1018 & 15498 & 29558 & 9113 & 252 \end{pmatrix},$$

$$F_{11}^e = \frac{1}{18018}\left(-6006, -75510, -15900, 85800, 11610, 6\right) u^e,$$

$$F_{12}^e = \frac{1}{18018}\left(-196479, -2640045, -762400, 3123360, 474915, 649\right) u^e,$$

$$F^e_{13} = \frac{1}{18018}(-586644, -8316700, -2956980, 10159260, 1697200, 3864)\, u^e,$$
$$F^e_{14} = \frac{1}{18018}(-277134, -4198800, -1855260, 5330580, 997050, 3564)\, u^e,$$
$$F^e_{15} = \frac{1}{18018}(-14814, -255690, -157760, 348300, 79470, 494)\, u^e,$$
$$F^e_{16} = \frac{1}{18018}(-3, -155, -300, 300, 155, 3)\, u^e,$$
$$F^e_{21} = \frac{1}{18018}(-196479, -2640045, -762400, 3123360, 474915, 649)\, u^e,$$
$$F^e_{22} = \frac{1}{18018}(-6900078, -105555450, -50414400, 135287940, 27405030, 176958)\, u^e,$$
$$F^e_{23} = \frac{1}{18018}(-21839788, -376504110, -256736460, 516367540, 136899000, 1813818)\, u^e,$$
$$F^e_{24} = \frac{1}{18018}(-11104728, -225391560, -223879220, 334775580, 122871300, 2728628)\, u^e,$$
$$F^e_{25} = \frac{1}{18018}(-687693, -19558365, -32766420, 32766420, 19558365, 687693)\, u^e,$$
$$F^e_{26} = \frac{1}{18018}(-494, -79470, -348300, 157760, 255690, 14814)\, u^e,$$
$$F^e_{31} = \frac{1}{18018}(-586644, -8316700, -2956980, 10159260, 1697200, 3864)\, u^e,$$
$$F^e_{32} = \frac{1}{18018}(-21839788, -376504110, -256736460, 516367540, 136899000, 1813818)\, u^e,$$
$$F^e_{33} = \frac{1}{18018}(-72572448, -1514993520, -1621139520, 2278115040, 907749120, 22841328)\, u^e,$$
$$F^e_{34} = \frac{1}{18018}(-39222888, -1065460520, -1757435280, 1757435280, 1065460520, 39222888)\, u^e,$$
$$F^e_{35} = \frac{1}{18018}(-2728628, -122871300, -334775580, 223879220, 225391560, 11104728)\, u^e,$$
$$F^e_{36} = \frac{1}{18018}(-3564, -997050, -5330580, 1855260, 4198800, 277134)\, u^e,$$
$$F^e_{41} = \frac{1}{18018}(-277134, -4198800, -1855260, 5330580, 997050, 3564)\, u^e$$
$$F^e_{42} = \frac{1}{18018}(-11104728, -225391560, -223879220, 334775580, 122871300, 2728628)\, u^e,$$
$$F^e_{43} = \frac{1}{18018}(-39222888, -1065460520, -1757435280, 1757435280, 1065460520, 39222888)\, u^e,$$
$$F^e_{44} = \frac{1}{18018}(-22841328, -907749120, -2278115040, 1621139520, 1514993520, 72572448)\, u^e,$$
$$F^e_{45} = \frac{1}{18018}(-1813818, -136899000, -516367540, 256736460, 376504110, 21839788)\, u^e,$$
$$F^e_{46} = \frac{1}{18018}(-3864, -1697200, -10159260, 2956980, 8316700, 586644)\, u^e,$$
$$F^e_{51} = \frac{1}{18018}(-14814, -255690, -157760, 348300, 79470, 494)\, u^e,$$
$$F^e_{52} = \frac{1}{18018}(-687693, -19558365, -32766420, 32766420, 19558365, 687693)\, u^e,$$
$$F^e_{53} = \frac{1}{18018}(-2728628, -122871300, -334775580, 223879220, 225391560, 11104728)\, u^e,$$
$$F^e_{54} = \frac{1}{18018}(-1813818, -136899000, -516367540, 256736460, 376504110, 21839788)\, u^e,$$
$$F^e_{55} = \frac{1}{18018}(-176958, -27405030, -135287940, 50414400, 105555450, 6900078)\, u^e,$$
$$F^e_{56} = \frac{1}{18018}(-649, -474915, -3123360, 762400, 2640045, 196479)\, u^e,$$

$$F_{61}^e = \frac{1}{18018}(-3, -155, -300, 300, 155, 3)\, u^e,$$
$$F_{62}^e = \frac{1}{18018}(-494, -79470, -348300, 157760, 255690, 14814)\, u^e,$$
$$F_{63}^e = \frac{1}{18018}(-3564, -997050, -5330580, 1855260, 4198800, 277134)\, u^e,$$
$$F_{64}^e = \frac{1}{18018}(-3864, -1697200, -10159260, 2956980, 8316700, 586644)\, u^e,$$
$$F_{65}^e = \frac{1}{18018}(-649, -474915, -3123360, 762400, 2640045, 196479)\, u^e,$$
$$F_{66}^e = \frac{1}{18018}(-6, -11610, -85800, 15900, 75510, 6006)\, u^e.$$
$$G_{11}^e = \frac{1}{46558512}(-11639628,-137732595,-20210190,150990840,18588570,3003)\, u^e,$$
$$G_{12}^e = \frac{1}{46558512}(-11364144666,-145988703105, -34353675930,168074933460,23613740340,17849901)\, u^e,$$
$$G_{13}^e = \frac{1}{46558512}(-98767822536, -1387033416220, -474031208120, 1683927719760,$$
$$275357605120, 547121996)\, u^e,$$
$$G_{14}^e = \frac{1}{46558512}(-22489923456,-364367075220,-192389448360,479713533120,99064906920,468006996)\, u^e,$$
$$G_{15}^e = \frac{1}{46558512}(-77212896,-1800939615,-1856355510,2810518080,913265430,10724511)\, u^e,$$
$$G_{16}^e = \frac{1}{46558512}(-126,-16165,-50930,35580,30640,1001)\, u^e,$$
$$G_{21}^e = \frac{1}{46558512}(-357596239,-4372632390,-789617120,4887048430,632593935,203384)\, u^e,$$
$$G_{22}^e = \frac{1}{46558512}(-380346297597,-5319019005300,-1826695356660,6453259150050, 1070015154705, 2786354802)\, u^e,$$
$$G_{23}^e = \frac{1}{46558512}(-3637831252252, -60786869005680, -37316523968240, 81855142247800,$$
$$19687822460940, 198259517432)\, u^e,$$
$$G_{24}^e = \frac{1}{46558512}(-970966024372, -22895214957480, -28822143475520, 36121117118920,$$
$$16137151825140, 430055513312)\, u^e,$$
$$G_{25}^e = \frac{1}{46558512}(-5083354467,-301437294570,-926962612920,573077684790,629039013435,31366563732)\, u^e,$$
$$G_{26}^e = \frac{1}{46558512}(-64249,-53933640,-352409420,88702330,295989285,21715694)\, u^e,$$
$$G_{31}^e = \frac{1}{46558512}(-1017550534,-12752760920,-2636616600,14461217980,1944782270,927804)\, u^e,$$
$$G_{32}^e = \frac{1}{46558512}(-1156967764962,-17393570992740,-7746795073200,22041373276500,4234600836210, 21359718192)\, u^e,$$
$$G_{33}^e = \frac{1}{46558512}(-11963292341592,-235252150803120,-215539837793280,344243739961200$$
$$, 116254087970520, 2257453006272)\, u^e,$$
$$G_{34}^e = \frac{1}{46558512}(-3632923392712,-121997997060320,-249600568750560,212751718739920,$$
$$156106920724520, 6372849739152)\, u^e,$$
$$G_{35}^e = \frac{1}{46558512}(-25546646382,-2866283736960,-12358558106760,5448764843340,9242102955990,559520690772)\, u^e,$$
$$G_{36}^e = \frac{1}{46558512}(-661914, -950114220, -6753146400,1395090180,5854994970,453837384)\, u^e,$$

$$G^e_{41} = \frac{1}{46558512}(\text{-}453837384,\text{-}5854994970,\text{-}1395090180,\ 6753146400,950114220,661914)\, u^e,$$
$$G^e_{42} = \frac{1}{46558512}(\text{-}559520690772,\text{-}9242102955990,\text{-}5448764843340,12358558106760,2866283736960,\ 25546646382)\, u^e,$$
$$G^e_{43} = \frac{1}{46558512}(\text{-}6372849739152,\ \text{-}156106920724520,\ \text{-}212751718739920,\ 249600568750560,$$
$$121997997060320, 3632923392712)\, u^e,$$
$$G^e_{44} = \frac{1}{46558512}(\text{-}2257453006272,\ \text{-}116254087970520,\ \text{-}344243739961200,215539837793280,$$
$$235252150803120, 11963292341592)\, u^e,$$
$$G^e_{45} = \frac{1}{46558512}(\text{-}21359718192,\text{-}4234600836210,\text{-}22041373276500,7746795073200,$$
$$17393570992740, 1156967764962)\, u^e,$$
$$G^e_{46} = \frac{1}{46558512}(\text{-}927804,\text{-}1944782270,\text{-}14461217980,2636616600,12752760920,1017550534)\, u^e,$$
$$G^e_{51} = \frac{1}{46558512}(\text{-}21715694,\ \text{-}295989285,\ \text{-}88702330,\ 352409420,\ 53933640,\ 64249)\, u^e,$$
$$G^e_{52} = \frac{1}{46558512}(-31366563732, -629039013435, -573077684790, 926962612920, 301437294570, 5083354467)\, u^e,$$
$$G^e_{53} = \frac{1}{46558512}(-430055513312, -16137151825140, -36121117118920, 28822143475520,$$
$$22895214957480, 970966024372)\, u^e,$$
$$G^e_{54} = \frac{1}{46558512}(-198259517432, -19687822460940, -81855142247800, 37316523968240,$$
$$60786869005680, 3637831252252)\, u^e,$$
$$G^e_{55} = \frac{1}{46558512}(-2786354802, -1070015154705, -6453259150050, 1826695356660,5319019005300, 380346297597)\, u^e,$$
$$G^e_{56} = \frac{1}{46558512}(-203384, -632593935, -4887048430, 789617120, 4372632390, 357596239)\, u^e,$$
$$G^e_{61} = \frac{1}{46558512}(-1001, -30640, -35580, 50930, 16165, 126)\, u^e,$$
$$G^e_{62} = \frac{1}{46558512}(-10724511, -913265430, -2810518080, 1856355510, 1800939615, 77212896)\, u^e,$$
$$G^e_{63} = \frac{1}{46558512}(-468006996, -99064906920, -479713533120, 192389448360, 364367075220, 22489923456)\, u^e,$$
$$G^e_{64} = \frac{1}{46558512}(-547121996, -275357605120, -1683927719760, 474031208120, 1387033416220, 98767822536)\, u^e,$$
$$G^e_{65} = \frac{1}{46558512}(-17849901, -23613740340, -168074933460, 34353675930, 145988703105, 11364144666)\, u^e,$$
$$G^e_{66} = \frac{1}{46558512}(-3003, -18588570, -150990840, 20210190, 137732595, 11639628)\, u^e.$$

$$D^e = \frac{1}{14h^2}\begin{pmatrix} -105 & 145 & 190 & -390 & 155 & 5 \\ -4485 & 3045 & 16710 & -23550 & 7215 & 1065 \\ -16990 & -5650 & 107940 & -120020 & 23770 & 10950 \\ -10950 & -23770 & 120020 & -107940 & 5650 & 16990 \\ -1065 & -7215 & 23550 & -16710 & -3045 & 4485 \\ -5 & -155 & 390 & -190 & -145 & 105 \end{pmatrix}.$$

9. Appendix B: An Algorithm for Undecadiagonal Matrices

Consider the following formulation of the N simulation equations solving problem [49]

$$[T]\{u\} = \{y\},$$

where $[T]$ is a matrix describing the coefficients of the equation and represent a vector of equations, $\{u\}$ represent the unknown equations and $\{y\}$ represent the known equations.

$$
M = \begin{bmatrix}
a_1 & b_1 & c_1 & d_1 & e_1 & f_1 & 0 & \cdots & \vdots & \vdots & \vdots & \vdots & \vdots & \vdots & 0 \\
g_2 & a_2 & b_2 & c_2 & d_2 & e_2 & f_2 & 0 & \cdots & \vdots & \vdots & \vdots & \vdots & \vdots & 0 \\
h_3 & g_3 & a_3 & b_3 & c_3 & d_3 & e_3 & f_3 & 0 & \cdots & \vdots & \vdots & \vdots & \vdots & 0 \\
m_4 & h_4 & g_4 & a_4 & b_4 & c_4 & d_4 & e_4 & f_4 & 0 & \cdots & \vdots & \vdots & \vdots & 0 \\
n_5 & m_5 & h_5 & g_5 & a_5 & b_5 & c_5 & d_5 & e_5 & f_5 & 0 & \cdots & \vdots & \vdots & 0 \\
p_6 & n_6 & m_6 & h_6 & g_6 & a_6 & b_6 & c_6 & d_6 & e_6 & f_6 & 0 & \cdots & \vdots & 0 \\
0 & p_7 & n_7 & m_7 & h_7 & g_7 & a_7 & b_7 & c_7 & d_7 & e_7 & f_7 & 0 & \cdots & 0 \\
\ddots & \ddots & \ddots & \ddots & \ddots & \ddots & \ddots & \ddots & \ddots & \ddots & \ddots & \ddots & \ddots & \ddots & \\
0 & \cdots & \vdots & 0 & p_{N-5} & n_{N-5} & m_{N-5} & h_{N-5} & g_{N-5} & a_{N-5} & b_{N-5} & c_{N-5} & d_{N-5} & e_{N-5} & f_{N-5} \\
0 & \vdots & \vdots & \cdots & 0 & p_{N-4} & n_{N-4} & m_{N-4} & h_{N-4} & g_{N-4} & a_{N-4} & b_{N-4} & c_{N-4} & d_{N-4} & e_{N-4} \\
0 & \vdots & \vdots & \vdots & \cdots & 0 & p_{N-3} & n_{N-3} & m_{N-3} & h_{N-3} & g_{N-3} & a_{N-3} & b_{N-3} & c_{N-3} & d_{N-3} \\
0 & \vdots & \vdots & \vdots & \vdots & \cdots & 0 & p_{N-2} & n_{N-2} & m_{N-2} & h_{N-2} & g_{N-2} & a_{N-2} & b_{N-2} & c_{N-2} \\
0 & \vdots & \vdots & \vdots & \vdots & \vdots & \cdots & 0 & p_{N-1} & n_{N-1} & m_{N-1} & h_{N-1} & g_{N-1} & a_{N-1} & b_{N-1} \\
0 & \vdots & \vdots & \vdots & \vdots & \vdots & \vdots & \cdots & 0 & p_N & n_N & m_N & h_N & g_N & a_N
\end{bmatrix}
$$

Applying LU decomposition, the 11-diagonal matrix is split into two tridiagonal matrices. Consequently, as required, define the ensuing parameters with forward recursion.

$$
\begin{aligned}
&q_1 = a_1, \quad r_1 = b_1, \quad s_1 = c_1, \quad t_1 = d_1, \quad \nu_1 = e_1, \quad z_2 = \frac{g_2}{q_1}, \\
&q_2 = a_2 - z_2 r_1, \quad r_2 = b_2 - z_2 s_1, \quad s_2 = c_2 - z_2 t_1, \\
&t_2 = d_2 - z_2 \nu_1, \quad \nu_2 = e_2 - z_2 f_1, \quad \alpha_3 = \frac{h_3}{q_1}, \quad z_3 = \frac{g_3 - \alpha_3 r_1}{q_2}, \\
&q_3 = a_3 - \alpha_3 s_1 - z_3 r_2, \quad r_3 = b_3 - \alpha_3 t_1 - z_3 s_2, \quad s_3 = c_3 - \alpha_3 \nu_1 - z_3 t_1, \\
&t_3 = d_3 - \alpha_3 f_1 - z_3 \nu_2, \quad \nu_3 = e_3 - z_3 f_2, \\
&\beta_4 = \frac{m_4}{q_1}, \quad \alpha_4 = \frac{h_4 - \beta_4 r_1}{q_2}, \quad z_4 = \frac{g_4 - \beta_4 s_1 - \alpha_4 r_2}{q_3}, \\
&q_4 = a_4 - \beta_4 t_1 - \alpha_4 s_2 - z_4 r_3, \quad r_4 = b_4 - \beta_4 \nu_1 - \alpha_4 t_2 - z_4 s_3, \\
&t_4 = d_4 - \alpha_4 f_2 - z_4 \nu_3, \quad \nu_4 = e_4 - z_4 f_3, \\
&\gamma_5 = \frac{\nu_5}{q_1}, \quad \beta_5 = \frac{m_5 - \gamma_5 r_1}{q_2}, \quad \alpha_5 = \frac{h_5 - \gamma_5 s_1 - \beta_5 r_2}{q_3}, \\
&z_5 = \frac{1}{q_4}\big(g_5 - \gamma_5 t_1 - \beta_5 s_2 - \alpha_5 r_3\big), \quad q_5 = a_5 - \gamma_5 \nu_1 - \beta_5 t_2 - \alpha_5 s_3 - z_5 r_4, \\
&r_5 = b_5 - \gamma_5 f_1 - \beta_5 \nu_2 - \alpha_5 t_3 - z_5 t_4, \quad s_5 = c_5 - \beta_5 f_2 - \alpha_5 \nu_3 - z_5 t_4, \\
&t_5 = d_5 - \alpha_5 f_3 - z_5 \nu_4, \quad \nu_5 = e_5 - z_5 f_4,
\end{aligned}
$$

and $i = 6 \to N$

$$
\begin{aligned}
&\epsilon_i = \frac{p_i}{q_{i-5}}, \quad \gamma_i = \frac{\nu_i - \epsilon_i r_{i-5}}{q_{i-4}}, \\
&\beta_i = \frac{1}{q_{i-3}}\big(m_i - \epsilon_i s_{i-5} - \gamma_i r_{i-4}\big), \quad \alpha_i = \frac{1}{q_{i-2}}\big(h_i - \epsilon_i t_{i-5} - \gamma_i s_{i-4} - \beta_i r_{i-3}\big),
\end{aligned}
$$

$$z_i = \frac{1}{q_{i-1}}\big(g_i - -\epsilon_i\nu_{i-5}\gamma_i t_{i-4} - \beta_i s_{i-3} - \alpha_i r_{i-2}\big),$$
$$q_i = a_i - \epsilon_i f_{i-5} - \gamma_i \nu_{i-4} - \beta_i t_{i-3} - \alpha_i s_{i-2} - z_i r_{i-1},$$
$$r_i = b_i - \gamma_i f_{i-4} - \beta_i \nu_{i-3} - \alpha_i t_{i-2} - z_i s_{i-1},$$
$$s_i = c_i - \beta_i f_{i-3} - \alpha_i \nu_{i-2} - z_i t_{i-1}, \quad , \quad t_i = d_i - \alpha_i f_{i-2} - z_i \nu_{i-1},$$
$$\nu_i = e_i - z_i f_{i-1}.$$

As a result, the vector $\{x\}$ can be determined from the lower tringular matrix.

$$x_1 = y_1 \quad , \quad x_2 = y_2 - z_2 x_1 \quad , \quad x_3 = y_3 - \alpha_3 x_1 - z_3 x_2,$$
$$x_4 = y_4 - \beta_4 x_1 - \alpha_4 x_2 - z_4 x_3 \quad , \quad x_5 = y_5 - y_5 x_1 - \beta_5 x_2 - \alpha_5 x_3 - z_5 x_4,$$

$i = 6 \to N$:

$$x_i = y_i - \epsilon_i x_{i-5} - \gamma_i x_{i-4} - \beta_i x_{i-3} - \alpha_i x_{i-2} - z_i x_{i-1}.$$

The unknown vector $\{u\}$ is subsequently computed from the upper triangular matrix using reverse recursion.

$$u_N = \frac{x_N}{q_N},$$
$$u_{N-1} = \frac{1}{q_{N-1}}\big(x_{N-1} - r_{N-1}u_N\big),$$
$$u_{N-2} = \frac{1}{q_{N-2}}\big(x_{N-2} - s_{N-2}u_N - r_{N-2}u_{N-1}\big),$$
$$u_{N-3} = \frac{1}{q_{N-3}}\big(x_{N-3} - t_{N-3}u_N - s_{N-3}u_{N-3} - r_{N-3}u_{N-2}\big),$$
$$u_{N-4} = \frac{1}{q_{N-4}}\big(x_{N-4} - \nu_{N-4}u_N - t_{N-4}u_{N-1} - s_{N-4}u_{N-2} - r_{N-4}u_{N-3}\big),$$

$i = (N-5) \to 1$

$$u_i = \frac{1}{q_i}\big(x_i - f_i u_{i+5} - \nu_i u_{i+4} - t_i u_{i+3} - s_i u_{i+2} - r_i u_{i+1}\big).$$

Acknowledgment

The author extend their appreciation to Prince Sattam bin Abdulaziz University for funding this research work through the project number (PSAU/2025/01/33017).

References

[1] I. L. Bogolubsky, *Some examples of inelastic soliton interaction*, J. Comp. Phys. Commun., *13* (1977), 149-155.

[2] P. G. Drazin and R. S. Johnson, *Solitons: an Introduction*, Cambridge University Press, 1989.

[3] D. J. Korteweg and G. De Vries, *On the change of form of long waves advancing in a rectangular canal and on a new type of long stationary wave*, Philosophical Magazine Series, *5* (1895), 422-443.

[4] T. Ak, S. Dhawan, S. B. G. Karakoc, S. K. Bhowmik, and K. R. Raslan, *Numerical study of rosenau-KdV equation using finite element method based on collocation approach*, Math. Modelling and Analy., *22*(3) (2017), 373-388.

[5] M. Ramadan, H. Samy, I. Hanafy, and W. Adel, *Petrov–Galerkin finite element method for solving the time-fractional Rosenau–Hyman equation*, J. of Umm Al-Qura University for Appl. Sci., (2025), 1-14.

[6] T. R. Marchant and N. F. Smyth, *The extended Korteweg-de Vries equation and the resonant flow of a fluid over topography*, J. of Fluid Mech., *221* (1990), 263-287.

[7] M. Ramadan and H. Aly, *New approach for solving of extended KdV equation*, Alfarama J. of Basic & Appl. Sci., *4*(1) (2023), 96-109.

[8] S. B. G. Karakoc and K. K. Ali, *New exact solutions and numerical approximations of the generalized KdV equation*, Comput. Meth. for Diff. Eq., *9*(3) (2021), 670-691.

[9] S. Ozer, *Two efficient numerical methods for solving Rosenau-KdV-RLW equation*, Kuwait J. of Sci., *48*(1) (2021), 14-24.

[10] A. Yokus, *Truncation and convergence dynamics: KdV Burgers model in the sense of Caputo derivative*, Boletim da Sociedade Paranaense de Matematica, *40* (2022), 1-7.

[11] D. Bai and L. Zhang, *The finite element method for the coupled Schrödinger–KdV equations*, Phys. Lett. A, *373*(26) (2009), 2237-2244.

[12] H. Samy, W. Adel, I. Hanafy, and M. Ramadan, *A Petrov-Galerkin approach for the numerical analysis of soliton and multi-soliton solutions of the Kudryashov-Sinelshchikov equation*, Iranian J. of Num. Anal. and Optim., *14*(4) (2024), 1309-1335.

[13] A. M. Kamchatnov, Y. H. Kuo, T. C. Lin, T. L. Horng, S. C. Gou, R. Clift, G. A. El, and R. H. J. Grimshaw, *Undular bore theory for the Gardner equation*, Physical Review E, *86* (2012), 036605/1-036605/23.

[14] K. R. Helfrich and W. K. Melville, *Long nonlinear internal waves*, Annu. Rev. Fluid Mech., *38* (2006), 395.

[15] J. R. Apel, L. A. Ostrovsky, Y. A. Stepanyants, and J. F. Lynch, *Internal solitons in the ocean and their effect on underwater sound*, J. Acoust. Soc. Am., *121* (2007), 695.

[16] H. Samy, W. Adel, I. Hanafy, and M. Ramadan, *A Petrov–Galerkin approach for the numerical analysis of soliton and multi-soliton solutions of the Kudryashov–Sinelshchikov equation*, Iranian J. of Num. Analy. and Optim., *14*(4) (2024), 1310-1335.

[17] Y. Edrisi Tabriz and M. Lakestani, *Direct solution of nonlinear constrained quadratic optimal control problems using B-spline functions*, Kybernetika, *51*(1) (2015), 81-98.

[18] R. Mohammadzadeh and M. Lakestani, *Optimal control of linear time-delay systems by a hybrid of block-pulse functions and biorthogonal cubic Hermite spline multiwavelets*, Optimal Control Applications and Methods, *39*(1) (2018), 357-376.

[19] M. Lakestani, *Numerical solutions of the KdV equation using B-spline functions*, Iranian Journal of Science and Technology, Transactions A: Science, *41*(2) (2017), 409-417.

[20] M. Lakestani, M. Razzaghi, and M. Dehghan, *Numerical solution of the controlled Duffing oscillator by semi-orthogonal spline wavelets*, Physica Scripta, *74*(3) (2006), 362-366.

[21] G. C. Das, *New method for rekindling the explosive waves in Maxwellian space plasmas*, Plasma Sci. and Tech., *22*(12) (2020), 125302.

[22] X. Pu and M. Li, *KdV limit of the hydromagnetic waves in cold plasma*, Zeitschrift für angewandte Mathematik und Physik, *70*(1) (2019), 1-16.

[23] S. A. El-Tantawy, A. H. Salas, and M. R. Alharthi, *A new approach for modelling the damped Helmholtz oscillator: applications to plasma physics and electronic circuits*, Commun. in Theoretical Phys., *73*(3) (2021), 35501.

[24] M. G. Hafez, *Nonlinear Schamel Korteweg-De Vries–Burgers equation to report ion-acoustic waves in the relativistic plasmas*, IEEE Transactions on Plasma Sci., *47*(12) (2019), 5314-5323.

[25] K. R. Helfrich and W. K. Melville, *Long nonlinear internal waves*, Annu. Rev. Fluid Mech., *38* (2006), 395-425.

[26] S. M. Ahmed, E. R. Hassib, U. M. Abdelsalam, R. E. Tolba, and W. M. Moslem, *Proliferation of soliton, explosive, shocklike, and periodic ion-acoustic waves in Titan's ionosphere*, Phys. of Plasmas, *27*(8) (2020), 82903.

[27] E. I. El-Awady, *Generation of freak waves in non-Maxwellian dusty plasmas in the domain of Gardner equation*, AstroPhys. and Space Sci., *364*(11) (2019), 1-7.

[28] S. A. El-Tantawy, A. T. Elgendy, and S. Ismail, *Cylindrical freak waves in a non-Maxwellian dusty bulk-sheath plasma: an approximate solution for the cylindrical nonlinear Schrödinger equation*, Phys. Lett. A, *381*(40) (2017), 3465-3471.

[29] N. H. Aljahdaly and S. A. El-Tantawy, *Simulation study on nonlinear structures in nonlinear dispersive media*, Chaos: An Interdisciplinary J. of Nonlinear Sci., *30*(5) (2020), 53117-53124.

[30] S.A. El-Tantawy, T. Aboelenen, and S.M.E. Ismaeel, *Local discontinuous Galerkin method for modeling the nonplanar structures (solitons and shocks) in an electronegative plasma*, Phys. of Plasmas, *26*(2) (2019), 22115-22122.

[31] S. A. El-Tantawy, A. H. Salas, M. Khalid, S. I. H. Bacha, and H. Al-Ghamdi, *The Tantawy technique for analyzing fractional Gardner equation and modeling fractional ion-acoustic solitary waves in electronegative plasmas*, Eur. Phys. J. D, *79* (2025), 156.

[32] M. Remoissenet, *Waves Called Solitons: Concepts and Experiments*, Springer, 1999.

[33] L. Degon and A. Chowdhury, *Approximate solutions to the Gardner equation by spectral modified exponential time differencing method*, Partial Diff. Eq. in Appl. Math., *5* (2022), 100310.

[34] K. A. Koroche and H. M. Chemeda, *Six-order compact finite difference method for solving KdV-Burger equation in the application of wave propagations*, Iranian J. of Num. Analy. and Optim., *27*(7) (2021), 1126-1138.

[35] A. Karczewska, P. Rozmej, M. Szczecinski, and B. Boguniewicz, *A finite element method for extended KdV equations*, Int. J. of Appl. Math. and Comp. Sci., *26*(3) (2016), 555-567.

[36] A. Yokus and H. Bulut, *Numerical simulation of KdV equation by finite difference method*, Indian J. of Phys., *92*(12) (2018), 1571-1575.

[37] M. M. Khader, K. M. Saad, Z. Hammouch, and D. Baleanu, *A spectral collocation method for solving fractional KdV and KdV-Burgers equations with non-singular kernel derivatives*, Appl. Num. Math., *161* (2021), 137-146.

[38] R. Grimshaw, D. Pelinovsky, E. Pelinovsky, and A. Slunyaev, *Generation of large-amplitude solitons in the extended Korteweg–de Vries equation*, Chaos: An Interdisciplinary J. of Nonlinear Sci., *12*(4) (2002), 1070-1076.

[39] E. I. El-Awady, *Generation of freak waves in non-Maxwellian dusty plasmas in the domain of Gardner equation*, Astrophys. and Space Sci., *364*(11) (2019), 1-7.

[40] K. Sowinski, *The Ritz method application for stress and deformation analyses of standard orthotropic pressure vessels*, Thin-Walled Structures, *162* (2021), 107585-107593.

[41] A. Al-Taweel and X. Wang, *The lowest-order stabilizer free weak Galerkin finite element method*, Appl. Num. Math., *157* (2020), 434-445.

[42] G. Y. Chen, M. Gan, S. Wang, and C. P. Chen, *Insights into algorithms for separable nonlinear least squares problems*, IEEE Transactions on Image Processing, *30* (2020), 1207-1218.

[43] N. K. Amein and M. A. Ramadan, *A small time solutions for the KdV equation using Bubnov-Galerkin finite element method*, J. of the Egyptian Math. Soci., *19* (2011), 118-125.

[44] H. Zureigat, M. A. Tashtoush, A. F. A. Jassar, E. A. Az-Zobi, and M. W. Alomari, *A solution of the complex fuzzy heat equation in terms of complex Dirichlet conditions using a modified Crank–Nicolson method*, Advances in Math. Phys., *2023* (2023), 1-8.

[45] J. Liu and Y. Hao, *Crank-Nicolson method for solving uncertain heat equation*, Soft Computing, *26*(3) (2022), 937-945.

[46] L. Degon and A. Chowdhury, *Approximate solutions to the Gardner equation by spectral modified exponential time differencing method*, Partial Diff. Eq. in Appl. Math., *5* (2022), 100310.

[47] E. Infeld, A. Karczewska, G. Rowlands, and P. Rozmej, *Exact cnoidal solutions of the extended KdV equation*, Acta Physica Polonica A, *133*(5) (2018), 1191-1199.

[48] O. E. Hepson, A. Korkmaz, and I. Dag, *Numerical solutions of the Gardner equation by extended form of the cubic B-splines*, Pramana, *91* (2018), 1-10.

[49] J. E. Halls and J. D. Wadhawan, *A model for efficient, semiconductor-free solar cells via supersensitized electron transfer cascades in photogalvanic devices*, Phys. Chemistry Chemical Phys., *15*(9) (2013), 3218-3226.